Robust Force Control of an SRM-Based Electromechanical Brake and Experimental Results

Prashanth Krishnamurthy, *Member, IEEE*, Wenzhe Lu, *Member, IEEE*, Farshad Khorrami, *Senior Member, IEEE*, and Ali Keyhani, *Fellow, IEEE*

***Abstract*—In this paper, we propose robust nonlinear force controllers for a switched-reluctance-motor (SRM) electromechanical brake system which is a promising replacement for hydraulic brakes in the automotive industry. A torque-level control law is first designed using robust backstepping. The backstepping proceeds via the force and the velocity states. The voltage-level control laws are obtained from the virtual control law for the torque using either an additional step of backstepping incorporating a novel voltage-commutation scheme or a torque-ripple-minimizing algorithm based on a design of turn-on/turn-off angles and torque factors. The controllers do not require knowledge of the motor mechanical parameters and the functional forms of the relationships among the motor position, the brake force, and the motor load torque. A detailed model of the motor including current-dependent inductance coefficients is used. The load exerted on the motor by the caliper may be modeled as a spring; however, the actual load model is taken to be an unknown nonlinear function of position to allow for uncertainties in the model. Hence, the developed controllers work for a wide variety of loads including brake systems. Moreover, the controllers provide significant robustness to uncertainty in the inductances and address practical current and voltage constraints. The performance of the proposed controllers is demonstrated through both simulation and experimental studies.**

***Index Terms*—Braking, electromechanical brake, force control, road vehicles, switched reluctance motor (SRM).**

I. Introduction

CONSIDERATIONS of safety, comfort, and fuel efficiency have encouraged the development of "by-wire" mechanisms [1] in the automotive industry over recent years; the ultimate goal of which is to enable any driver to be as "skillful" in maneuvering and stabilizing the car as a professional driver. One such system is the electromechanical brake system [2]–[4] used to replace hydraulic brakes. Brake systems in an automobile are shown in Fig. 1. A cross section of a brake system showing the motor and the caliper is shown in Fig. 2. The driver's foot pressure measured by a sensor on the brake pedal is communicated to microcontrollers that relay the signal to the electromechanical brake actuators situated at each wheel. The brake actuators then apply the required pressure at the brake pads to smoothly control the car's speed. This is in contrast to a conventional car in which a hydraulic system would directly respond to pressure on the brake pedal to apply pressure to the brake pads. A popular actuator used in brake systems and other electric-vehicle applications is the switched reluctance motor (SRM) [5]–[7]. Considerable effort on design [8]–[10] and modeling [11]–[16] of SRMs has been reported in the literature. Position and speed control of SRMs has been considered in [17]–[25]. A torque-ripple controller using iterative learning was designed in [26]. A torque-ripple controller based on an outer loop PI speed controller and an inner loop fuzzy-logic direct-drive controller with current chopping was proposed in [27]. A neural-network-based torque controller was designed in [28] while a force controller based on numerically inverting the torque–current relation using a look-up table was proposed in [29]. The problem of determining optimal turn-on and turn-off firing angles for maximizing efficiency in single-pulse-controlled SRM drives was addressed in [30]. Modeling and control of radial force in an SRM were considered in [31]. A sliding-mode observer for position and speed estimation in SRM drives was proposed in [32].

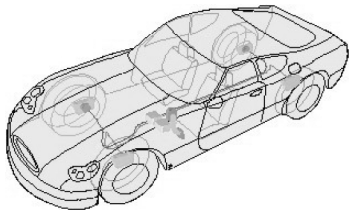

Fig. 1. Brake systems in an automobile (from [1]).

In this paper, we develop new robust nonlinear force controllers for an SRM-based electromechanical brake system (Fig. 3). We utilize a detailed model of the motor, including current dependence of the inductance coefficients. The load is taken to be an unknown nonlinear function of position. The modeling and problem statement are contained inSection II. The controller design is provided in Section III. A robust-backstepping [33] design is used to create a desired torque command from which voltage-level control laws are obtained using either another step of robust backstepping based on a novel voltage-commutation scheme or a torque-ripple-minimizing

Manuscript received January 09, 2006; revised July 23, 2007 and January 25, 2008. Manuscript received in final form September 25, 2008. First published April 17, 2009; current version published October 23, 2009. Recommended by Associate Editor C. Bohn. The work of P. Krishnamurthy and F. Khorrami was supported in part by the NSF under Grants ECS0105320 and ECS0501539. The work of W. Lu and A. Keyhani was supported in part by the NSF under Grant ECS0501349 and in part by the Department of Electrical and Computer Engineering Mechatronic–Green Energy Systems Laboratory, The Ohio State University. An earlier version of this paper was presented at the IEEE Conference on Decision and Control, Seville, Spain, Dec. 2005.

P. Krishnamurthy is with the IntelliTech Microsystems, Inc., Bowie, MD 20715 USA.

W. Lu is with the Vanner Inc., Hilliard, OH 43026 USA.

F. Khorrami is with the Control/Robotics Research Laboratory, Department of Electrical and Computer Engineering, Polytechnic University, Brooklyn, NY 11201 USA.

A. Keyhani is with the Department of Electrical and Computer Engineering, The Ohio State University, Columbus, OH 43210 USA.

Digital Object Identifier 10.1109/TCST.2008.2006908

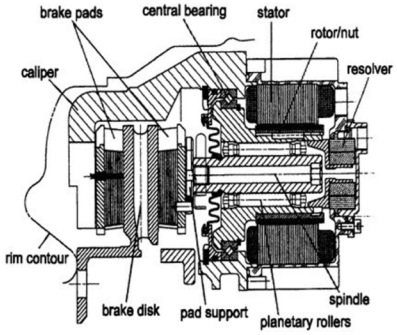

Fig. 2. Cross section of a brake system (from [2]).

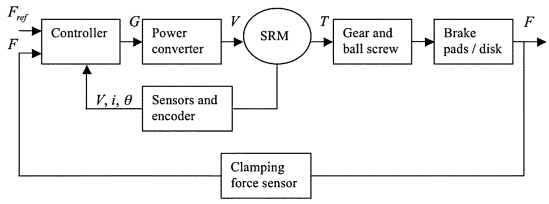

Fig. 3. Block diagram of clamping-force controller in an electromechanical brake system.

algorithm based on a design of turn-on/turn-off angles and torque factors. The controllers do not require knowledge of the motor mechanical parameters and the functional forms of the relationships among motor position, brake force, and motor load torque. Moreover, the controllers provide significant robustness to uncertainty in inductances. The experimental setup at the Mechatronics Laboratory of The Ohio State University is described in Section IV. The performance and robustness of the proposed controllers are demonstrated through simulation and experimental studies in Sections V and VI, respectively.

II. Modeling and Problem Statement

The dynamic model [11]–[16], [24] of an SRM-based electromechanical system can be written in terms of the SRM mechanical dynamics, the SRM electrical dynamics, and the brake characteristics, as described further in this section. The SRM mechanical dynamics are given by

$$J\ddot{\theta} = \tau - D\omega - \tau_L \tag{1}$$

where J is the rotational inertia of the motor, D is the viscous friction coefficient, θ is the motor position, ω is the velocity, τ_L is the load torque, and τ is the generated electromechanical torque. The total electromechanical torque τ is given by

$$\tau = \sum_{j=1}^{N} \tau_j(\theta, i_j) \tag{2}$$

where N is the number of phases, τ_j is the torque contribution of the jth phase, andi_j is the current in the jth phase. The torque τ_j is given by

$$\tau_j(\theta, i_j) = \int_0^{i_j} \frac{\partial L_j(\theta, i)}{\partial \theta} i \mathrm{d}i \tag{3}$$

where L_j is the inductance associated with the jth phase. The phase inductance L_j is, in general, nonlinear but periodic in θ. Hence, it can be represented as a Fourier series in θ with coefficients being functions of i_j. Retaining, for instance, the first three terms of the Fourier series expansion, we obtain

$$L_j(\theta, i_j) = \sum_{k=0}^{2} L_{k,j}(i_j) \cos\left(kN_r\left(\theta - (j-1)\frac{2\pi}{NN_r}\right)\right) \tag{4}$$

where N_r is the number of rotor poles. Defining $L_{a,j}(i_j)$ to be the inductance at aligned position, L_u to be the inductance at the unaligned position,[1] and $L_{m,j}(i_j)$ to be the inductance at the midway position (between aligned and unaligned)

$$\begin{aligned} L_{a,j}(i_j) &= L_{0,j}(i_j) + L_{1,j}(i_j) + L_{2,j}(i_j) \\ L_u &= L_{0,j}(i_j) - L_{1,j}(i_j) + L_{2,j}(i_j) \\ L_{m,j}(i_j) &= L_{0,j}(i_j) - L_{2,j}(i_j). \end{aligned} \tag{5}$$

Hence

$$\begin{aligned} L_{0,j}(i_j) &= \frac{1}{2}\left[\frac{1}{2}(L_{a,j}(i_j) + L_u) + L_{m,j}(i_j)\right] \\ L_{1,j}(i_j) &= \frac{1}{2}[L_{a,j}(i_j) - L_u] \\ L_{2,j}(i_j) &= \frac{1}{2}\left[\frac{1}{2}(L_{a,j}(i_j) + L_u) - L_{m,j}(i_j)\right]. \end{aligned} \tag{6}$$

The inductance coefficients $L_{a,j}(i_j)$ and $L_{m,j}(i_j)$ are modeled as polynomial functions of the current i_j

$$L_{a,j}(i_j) = \sum_{n=0}^{k} a_n i_j^n \qquad L_{m,j}(i_j) = \sum_{n=0}^{k} b_n i_j^n \tag{7}$$

where k is a nonnegative integer. With the inductance model developed earlier, the torque expression given in (3) reduces to

$$\begin{aligned} \tau_j(\theta, i_j) = -\frac{N_r}{4} i_j^2 \Bigg[& (L_{a,j}^{**}(i_j) - L_u) \\ & \times \sin\left(N_r\left(\theta - (j-1)\frac{2\pi}{NN_r}\right)\right) \\ & + (L_{a,j}^{**}(i_j) + L_u - 2L_{m,j}^{**}(i_j)) \\ & \times \sin\left(2N_r\left(\theta - (j-1)\frac{2\pi}{NN_r}\right)\right)\Bigg] \end{aligned} \tag{8}$$

where

$$\begin{aligned} L_{a,j}^{**}(i_j) &= \sum_{n=0}^{k} \frac{2}{n+2} a_n i_j^n \\ L_{m,j}^{**}(i_j) &= \sum_{n=0}^{k} \frac{2}{n+2} b_n i_j^n. \end{aligned} \tag{9}$$

The electrical dynamics of the SRM are given by

$$v_j = Ri_j + \frac{\mathrm{d}}{\mathrm{d}t}\lambda_j(\theta, i_j) \tag{10}$$

[1]Since the machine is unsaturated at the unaligned position, L_u is a constant (independent of i_j).

where v_j and λ_j are the voltage and flux, respectively, associated with the jth phase and R is the phase resistance. Using $\lambda_j(\theta, i_j) = L_j(\theta, i_j) i_j$, we obtain

$$v_j = Ri_j + L_j \frac{\mathrm{d}i_j}{\mathrm{d}t} + i_j \left(\frac{\partial L_j}{\partial \theta}\omega + \frac{\partial L_j}{\partial i_j}\frac{\mathrm{d}i_j}{\mathrm{d}t} \right). \tag{11}$$

Hence

$$\frac{\mathrm{d}i_j}{\mathrm{d}t} = \frac{1}{\left(L_j + i_j \frac{\partial L_j}{\partial i_j} \right)} \left[v_j - Ri_j - i_j \frac{\partial L_j}{\partial \theta}\omega \right]. \tag{12}$$

From physical considerations, it is meaningful to assume that the denominator in (12) is positive within the range of operation of the motor, i.e.,

$$L_j + i_j \frac{\partial L_j}{\partial i_j} > \epsilon > 0. \tag{13}$$

Using the inductance model (4)

$$\begin{aligned} \frac{\partial L_j}{\partial \theta} = -\frac{N_r}{2} \Bigg[& (L_{a,j} - L_u) \\ & \times \sin\left(N_r \left(\theta - (j-1)\frac{2\pi}{NN_r} \right) \right) \\ & + (L_{a,j} + L_u - 2L_{m,j}) \\ & \times \sin\left(2N_r \left(\theta - (j-1)\frac{2\pi}{NN_r} \right) \right) \Bigg] \end{aligned}$$

$$\begin{aligned} L_j + i_j \frac{\partial L_j}{\partial i_j} = & \frac{1}{2}\left[\frac{1}{2}(L^*_{a,j} + L_u) + L^*_{m,j} \right] \\ & + \frac{1}{2}(L^*_{a,j} - L_u) \\ & \times \cos\left(N_r \left(\theta - (j-1)\frac{2\pi}{NN_r} \right) \right) \\ & + \frac{1}{2}\left[\frac{1}{2}(L^*_{a,j} + L_u) - L^*_{m,j} \right] \\ & \times \cos\left(2N_r \left(\theta - (j-1)\frac{2\pi}{NN_r} \right) \right) \end{aligned} \tag{14}$$

where $L^*_{a,j}(i_j) = \sum_{n=0}^{k}(n+1)a_n i_j^n$ and $L^*_{m,j}(i_j) = \sum_{n=0}^{k}(n+1)b_n i_j^n$. The load torque τ_L seen by the motor is, in general, a nonlinear function of the actuator force F applied at the brake. The dependence of load torque on actuator force and the dependence of actuator force on motor mechanical variables are governed by the mechanical coupling between the motor and the load. In general, F and τ_L are given by$F = \mu_F(\theta)$ and $\tau_L = \mu_L(F)$, where μ_F and μ_L are nonlinear functions. Physically, it is meaningful to assume that μ_F is monotonic and that the slope of the function μ_F is positive and bounded, i.e.,[2]

$$\underline{\mu}_F \le \frac{\partial \mu_F}{\partial \theta} \le \overline{\mu}_F. \tag{15}$$

Furthermore, typically, τ_L is proportional to F with the proportionality constant being essentially the gear ratio of the coupling between the motor shaft and the load. For generality, however, we only require that

$$|\tau_L| \le \overline{\mu}_L |F| + \hat{\mu}_L \tag{16}$$

where $\overline{\mu}_L$ and $\hat{\mu}_L$ are nonnegative constants.

The control objective is to make F track a given reference trajectory F_{ref}. Practically, it is reasonable to consider F_{ref} and its first derivative to be bounded almost everywhere.

III. Controller Design

The controller design proposed in this paper consists of two parts. In the first part of the controller design (see Section III-A), a desired torque signal is generated using robust backstepping. In the second part of the controller design, voltage-level control laws are obtained from the desired torque command using either another step of robust backstepping (see Section III-B) or a torque-ripple-minimizing algorithm (see Section III-C).

A. Robust-Backstepping-Based Design of Torque-Level Control Law

In this section, a torque-level control law for the SRM brake system is designed using robust backstepping. The backstepping design proceeds by considering lower dimensional subsystems and designing *virtual* control inputs (or equivalently, state transformations). In the first step of backstepping, the 1-D system $\dot{F} = (\partial \mu_F / \partial \theta)\omega$ is considered, and ω is regarded as the virtual control input. Choosing $\omega = -k_1 z_1 = -k_1(F - F_{\mathrm{ref}})$ would result in practical tracking. However, since ω is not the actual control input, the error between ω and the *desired*ω is formulated as z_2. In the second step of backstepping, the torque τ will be regarded as the virtual control input and will be *designed* to make z_2 small, i.e., to make ω converge to the virtual control law ω^* and, hence, to make F converge to F_{ref}. However, since τ is also not the actual control input, the process should be repeated once more (see Section III-B) by introducing an error z_3 which is the difference between τ and the *desired*τ. At the third step of backstepping, the control inputs $v_j, j = 1, \ldots, N$ appear, and the control law that is designed at that step can be implemented. Alternatively, the torque-level control law obtained after the second step of backstepping can be converted into a voltage-level control law using a torque-ripple-minimizing algorithm (see Section III-C).

Step 1: Define a Lyapunov function $V_1 = (1/2)z_1^2$ where

$$z_1 = F - F_{\mathrm{ref}} \tag{17}$$

is the force tracking error. Differentiating V_1, we obtain

$$\begin{aligned} \dot{V}_1 = z_1(\dot{F} - \dot{F}_{\mathrm{ref}}) &= z_1 \left(\frac{\partial \mu_F}{\partial \theta}\omega - \dot{F}_{\mathrm{ref}} \right) \\ &= -k_1 \frac{\partial \mu_F}{\partial \theta} z_1^2 + z_1 z_2 \frac{\partial \mu_F}{\partial \theta} - z_1 \dot{F}_{\mathrm{ref}} \end{aligned} \tag{18}$$

where

$$z_2 = \omega - \omega^*, \qquad \omega^* = -k_1 z_1 \tag{19}$$

and $k_1 > 0$ is a design freedom. Using (15), (18) reduces to

$$\dot{V}_1 \le -k_1 \underline{\mu}_F z_1^2 + \overline{\mu}_F |z_1||z_2| + |z_1||\dot{F}_{\mathrm{ref}}|. \tag{20}$$

Step 2: Defining a new Lyapunov function $V_2 = V_1 + [1/(2c_2)]z_2^2$, where $c_2 > 0$ is a design parameter, we obtain

[2]Without loss of generality, we have assumed that μ_F is monotonically increasing.

Please keep text here

$$
\begin{aligned}
&\le -k_1\underline{\mu}_F z_1^2 + \overline{\mu}_F|z_1||z_2| + |z_1||\dot{F}_{\rm ref}| \\
&\quad + \frac{1}{c_2}z_2\left[\frac{1}{J}(\tau - D\omega - \tau_L) + k_1\frac{\partial \mu_F}{\partial \theta}\omega - k_1\dot{F}_{\rm ref}\right] \\
&\le -k_1\underline{\mu}_F z_1^2 + \overline{\mu}_F|z_1||z_2| + |z_1||\dot{F}_{\rm ref}| - \frac{k_2}{Jc_2}z_2^2 \\
&\quad + \frac{1}{Jc_2}|z_2||z_3| + \frac{D}{Jc_2}|z_2|[|z_2| + k_1|z_1|] \\
&\quad + \frac{1}{Jc_2}|z_2|[\overline{\mu}_L(|z_1| + |F_{\rm ref}|) + \hat{\mu}_L] \\
&\quad + \frac{k_1}{c_2}\overline{\mu}_F|z_2|[|z_2| + k_1|z_1|] + \frac{k_1}{c_2}|z_2||\dot{F}_{\rm ref}| \qquad (21)
\end{aligned}
$$

where

$$
\begin{aligned}
z_3 &= \tau - \tau^* \\
\tau^* &= -k_2 z_2 = -k_2[\omega + k_1(F - F_{\rm ref})] \qquad (22)
\end{aligned}
$$

where $k_2 > 0$ is a controller gain picked by the designer.

B. Robust-Backstepping-Based Design of Voltage-Level Control Law

The torque-level control law obtained in Section III-A can be converted into a voltage-level control law using a third step of backstepping. To perform this step of backstepping, we need the dynamics of the torque which can be derived using (8) as

$$
\begin{aligned}
\dot{\tau} &= \sum_{j=1}^{N}\dot{\tau}_j \qquad (23) \\
\dot{\tau}_j &= \frac{\partial \tau_j}{\partial \theta}\omega + \frac{\partial \tau_j}{\partial i_j}\dot{i}_j \\
&= \frac{\partial \tau_j}{\partial \theta}\omega + \frac{\frac{\partial \tau_j}{\partial i_j}\left[v_j - Ri_j - i_j\frac{\partial L_j}{\partial \theta}\omega\right]}{\left(L_j + i_j\frac{\partial L_j}{\partial i_j}\right)} \qquad (24)
\end{aligned}
$$

where

$$
\begin{aligned}
\frac{\partial \tau_j}{\partial \theta} &= -\frac{N_r^2}{4}i_j^2\Bigg[(L_{a,j}^{**} - L_u) \\
&\qquad \times \cos\left(N_r\left(\theta - (j-1)\frac{2\pi}{NN_r}\right)\right) \\
&\qquad + 2(L_{a,j}^{**} + L_u - 2L_{m,j}^{**}) \\
&\qquad \times \cos\left(2N_r\left(\theta - (j-1)\frac{2\pi}{NN_r}\right)\right)\Bigg] \qquad (25) \\
\frac{\partial \tau_j}{\partial i_j} &= -\frac{N_r}{2}i_j\Bigg[(L_{a,j}^{**} - L_u) \\
&\qquad \times \sin\left(N_r\left(\theta - (j-1)\frac{2\pi}{NN_r}\right)\right) \\
&\qquad + (L_{a,j}^{**} + L_u - 2L_{m,j}^{**}) \\
&\qquad \times \sin\left(2N_r\left(\theta - (j-1)\frac{2\pi}{NN_r}\right)\right)\Bigg] \\
&\quad - \frac{N_r}{4}i_j^2\Bigg[\frac{\partial L_{a,j}^{**}}{\partial i_j}\sin\left(N_r\left(\theta - (j-1)\frac{2\pi}{NN_r}\right)\right) \\
&\quad + \left(\frac{\partial L_{a,j}^{**}}{\partial i_j} - 2\frac{\partial L_{m,j}^{**}}{\partial i_j}\right) \\
&\quad \times \sin\left(2N_r\left(\theta - (j-1)\frac{2\pi}{NN_r}\right)\right)\Bigg]. \qquad (26)
\end{aligned}
$$

The third and final step of backstepping is carried out using the Lyapunov function $V_3 = V_2 + [1/(2c_3)]z_3^2$, where $c_3 > 0$ is a design freedom. Differentiating V_3 and using (21), we have

$$
\begin{aligned}
\dot{V}_3 &\le -k_1\underline{\mu}_F z_1^2 + \overline{\mu}_F|z_1||z_2| + |z_1||\dot{F}_{\rm ref}| - \frac{k_2}{Jc_2}z_2^2 \\
&\quad + \frac{1}{Jc_2}|z_2||z_3| + \frac{D}{Jc_2}|z_2|[|z_2| + k_1|z_1|] \\
&\quad + \frac{1}{Jc_2}|z_2|[\overline{\mu}_L(|z_1| + |F_{\rm ref}|) + \hat{\mu}_L] \\
&\quad + \frac{k_1}{c_2}\overline{\mu}_F|z_2|[|z_2| + k_1|z_1|] + \frac{k_1}{c_2}|z_2||\dot{F}_{\rm ref}| \\
&\quad + \frac{1}{c_3}z_3\left[\hat{\tau} + k_2\left(\frac{1}{J}(\tau - D\omega - \tau_L)\right.\right. \\
&\qquad \left.\left. + k_1\frac{\partial \mu_F}{\partial \theta}\omega - k_1\dot{F}_{\rm ref}\right)\right] \qquad (27)
\end{aligned}
$$

where, for notational convenience, we have introduced $\hat{\tau} = \dot{\tau}$. The control law will first be designed in terms of $\hat{\tau}$. The control laws in terms of the input voltages v_j will then be obtained through a commutation scheme. Designing

$$
\hat{\tau} = -k_3 z_3 = -k_3\left[\tau + k_2\omega + k_2k_1(F - F_{\rm ref})\right] \qquad (28)
$$

where $k_3 > 0$ is a design freedom, (27) reduces to

$$
\begin{aligned}
\dot{V}_3 &\le -k_1\underline{\mu}_F z_1^2 + \overline{\mu}_F|z_1||z_2| + |z_1||\dot{F}_{\rm ref}| - \frac{k_2}{Jc_2}z_2^2 \\
&\quad + \frac{1}{Jc_2}|z_2||z_3| + \frac{D}{Jc_2}|z_2|[|z_2| + k_1|z_1|] \\
&\quad + \frac{1}{Jc_2}|z_2|[\overline{\mu}_L(|z_1| + |F_{\rm ref}|) + \hat{\mu}_L] \\
&\quad + \frac{k_1}{c_2}\overline{\mu}_F|z_2|[|z_2| + k_1|z_1|] + \frac{k_1}{c_2}|z_2||\dot{F}_{\rm ref}| - \frac{k_3}{c_3}z_3^2 \\
&\quad + \frac{k_2}{Jc_3}|z_3|[|z_3| + k_2|z_2|] + \frac{k_2D}{Jc_3}|z_3|[|z_2| + k_1|z_1|] \\
&\quad + \frac{k_2}{Jc_3}|z_3|[\overline{\mu}_L(|z_1| + |F_{\rm ref}|) + \hat{\mu}_L] \\
&\quad + \frac{k_1k_2}{c_3}\overline{\mu}_F|z_3|[|z_2| + k_1|z_1|] + \frac{k_1k_2}{c_3}|z_3||\dot{F}_{\rm ref}| \qquad (29) \\
&= -k_1\underline{\mu}_F z_1^2 - \frac{k_2}{Jc_2}z_2^2 - \frac{k_3}{c_3}z_3^2 \\
&\quad + |z_1||z_2|\left[\overline{\mu}_F + \frac{k_1D}{Jc_2} + \frac{\overline{\mu}_L}{Jc_2} + \frac{k_1^2\overline{\mu}_F}{c_2}\right] \\
&\quad + |z_1||z_3|\left[\frac{k_1k_2D}{Jc_3} + \frac{k_2\overline{\mu}_L}{Jc_3} + \frac{k_1^2k_2\overline{\mu}_F}{c_3}\right] \\
&\quad + |z_2||z_3|\left[\frac{1}{Jc_2} + \frac{k_2^2}{Jc_3} + \frac{k_2D}{Jc_3} + \frac{k_1k_2\overline{\mu}_F}{c_3}\right] \\
&\quad + z_2^2\left[\frac{D}{Jc_2} + \frac{k_1\overline{\mu}_F}{c_2}\right] + z_3^2\left[\frac{k_2}{Jc_3}\right] + |z_1||\dot{F}_{\rm ref}| \\
&\quad + \frac{\overline{\mu}_L}{Jc_2}|z_2||F_{\rm ref}| + \frac{k_2\overline{\mu}_L}{Jc_3}|z_3||F_{\rm ref}| + \frac{\hat{\mu}_L}{Jc_2}|z_2|
\end{aligned}
$$

Can you keep this end of the eq with the others?

$$+\frac{\kappa_1}{c_2}|z_2||\dot{F}_{\rm ref}|+\frac{\kappa_2\mu_L}{Jc_3}|z_3|+\frac{\kappa_1\kappa_2}{c_3}|z_3||\dot{F}_{\rm ref}|. \quad (30)$$

From (30), it is seen that by picking k_1, k_2, k_3, c_2, and c_3 appropriately, V_3 satisfies

$$\dot{V}_3 \le -\gamma V_3 + \chi\left[F_{\rm ref}^2+\dot{F}_{\rm ref}^2+\hat{\mu}_L^2\right] \quad (31)$$

where $\gamma=\min(k_1\underline{\mu}_F, k_2/J, k_3)$ and χ is a constant independent of the controller gains k_1, k_2, and k_3. The proof of (31) follows by quadratic overbounding which is standard in the backstepping literature [24], [33] and is omitted here for brevity. From (31), it follows that practical tracking is achieved, i.e., the force tracking error $z_1=F-F_{\rm ref}$ can be regulated to an arbitrarily small compact set by picking k_1, k_2, and k_3 large enough.

To obtain control laws in terms of the input voltages $v_j, j=1,\ldots,N$, to achieve the designed form of $\hat{\tau}$ in (28), the following commutation scheme is used

$$v_j=\left(L_j+i_j\frac{\partial L_j}{\partial i_j}\right)\tilde{v}_j+Ri_j+i_j\frac{\partial L_j}{\partial\theta}\omega \quad (32)$$

$$\tilde{v}_j=\frac{\frac{\partial\tau_j}{\partial i_j}\left[\hat{\tau}-\sum_{n=1}^{N}\frac{\partial\tau_n}{\partial\theta}\omega\right]}{\sum_{n=1}^{N}\left(\frac{\partial\tau_n}{\partial i_n}\right)^2}. \quad (33)$$

From (33)

$$\sum_{j=1}^{N}\tilde{v}_j\frac{\partial\tau_j}{\partial i_j}=\hat{\tau}-\sum_{j=1}^{N}\frac{\partial\tau_j}{\partial\theta}\omega. \quad (34)$$

The commutation scheme (33) exhibits a singularity when all the currents are zero, i.e., when $i_1=\cdots=i_N=0$. Since the torque vanishes when all the currents are zero, this singularity is not encountered during normal operation of the motor. However, the commutation scheme must be slightly altered during the initial transient when the motor is powered on. This is done by using the standard technique of incorporating a small positive constant ϵ_τ into the denominator to yield the commutation law

$$\tilde{v}_j=\frac{\frac{\partial\tau_j}{\partial i_j}\left[\hat{\tau}-\sum_{n=1}^{N}\frac{\partial\tau_n}{\partial\theta}\omega\right]}{\sum_{n=1}^{N}\left(\frac{\partial\tau_n}{\partial i_n}\right)^2+\epsilon_\tau}. \quad (35)$$

The overall controller is given by (17), (19), (22), (28), (32), and (35). The controller design freedoms are k_1, k_2, k_3, c_2, and c_3. Noting the structure of the controller, the control law can be slightly generalized to provide additional damping in the electrical dynamics and to provide more design freedom in shaping the force dynamics. The generalized control law is given by

$$\hat{\tau}=-K_p(F-F_{\rm ref})-K_d(\dot{F}-\dot{F}_{\rm ref}) - K_i\int_0^t(F(t_1)-F_{\rm ref}(t_1))\mathrm{d}t_1-K_\tau\tau-K_\omega\omega \quad (36)$$

$$\tilde{v}_j=\frac{\frac{\partial\tau_j}{\partial i_j}\left[\hat{\tau}-\sum_{n=1}^{N}\frac{\partial\tau_n}{\partial\theta}\omega\right]}{\sum_{n=1}^{N}\left(\frac{\partial\tau_n}{\partial i_n}\right)^2+\epsilon_\tau} \quad (37)$$

$$v_j=\left(L_j+i_j\frac{\partial L_j}{\partial i_j}\right)\tilde{v}_j+i_j\frac{\partial L_j}{\partial\theta}\omega-K_{\rm cur}i_j \quad (38)$$

where K_p, K_d, K_i, K_τ, K_ω, and $K_{\rm cur}$ are controller gains free to be picked by the designer.

In the practical implementation of the controller, certain voltage and current constraints must be addressed. Typical voltage constraints include either a limited range or even a finite number of achievable voltages. For instance, the switching circuits typically used to drive SRMs provide only $\pm v_{\max}$, where $v_{\max}$ is a positive voltage. To handle such a voltage constraint, the control law (38) must be saturated, and a pulsewidth-modulation (PWM) scheme must be utilized. The choice of the PWM waveform period must take into account the switching frequency of the SRM driving circuit. This also entails a tradeoff among the PWM waveform period, the bandwidth of the closed loop, and the number of bits of resolution that the PWM scheme achieves.

Practically, the currents are also constrained to lie in a limited range depending on the amplifiers used to drive the motor. To handle this constraint, the voltages are redesigned to include a current-regulation regime. When any of the currents i_j exceeds a certain limit $i_{\max}$, the corresponding voltage v_j is switched from (38) to

$$v_j=-v_{\max}\mathrm{sign}(i_j), \qquad \text{if } |i_j|>i_{\max}. \quad (39)$$

A similar scheme is used around $i_j=0$ if the current is constrained to remain positive (as is usually the case due to the use of unipolar amplifiers).

Note that the controller design does not require the knowledge of the mechanical parameters D and J of the motor. In addition, the functional form of $F=\mu_F(\theta)$ and $\tau_L=\mu_L(F)$ are not required to be known. Magnitude bounds on D, J, μ_F, and μ_L are sufficient for picking the controller gains. While the controller utilizes nominal knowledge of the electrical parameters of the motor, the design does provide considerable robustness to uncertainty in the electrical parameters also as demonstrated through simulations in Section V.

C. Torque-Ripple-Minimizing Voltage-Level Control Law

An alternative would be to commutate the desired torque τ^* into the currents i_j using (2) and (8). To get the desired clamping-force response, the SRM in the electromechanical brake system needs to be operated in all four quadrants of the torque–speed plane. At the same time, the ripple in the torque generated by the SRM must be minimized to reduce acoustic noise and mechanical vibration. The rotating direction (or the sign of the speed ω) of the SRM is determined by the exciting sequence. The working mode of the SRM (motoring or generating or the sign of the torque τ) is determined by the conduction angle. The SRM is operating in motoring mode when the phases are conducting in inductance-ascending region and in generating mode when the phases are conducting in inductance-descending region.

With the phase current i held fixed, the torque profile (of an 8/6 SRM) is shown in Fig. 4. It is clear that high torque is not available near aligned or unaligned positions even when a high phase current is applied. To generate a ripple-free output torque, there must be overlapping among phases. During phase overlapping, the torque generated in one phase is decreasing and that in

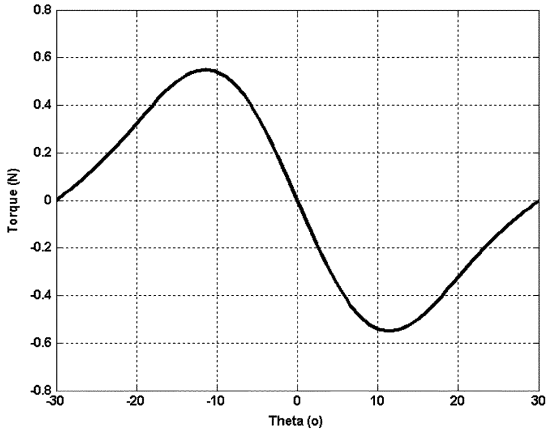

Fig. 4. Phase torque profile under fixed current.

TABLE I
TURN-ON/TURN-OFF ANGLES FOR PHASE A

	Quadrant I	Quadrant II	Quadrant III	Quadrant IV
$\theta_{on,A}$	-30^o	5^o	7.5^o	-27.5^o
$\theta_{off,A}$	-7.5^o	27.5^o	30^o	-5^o

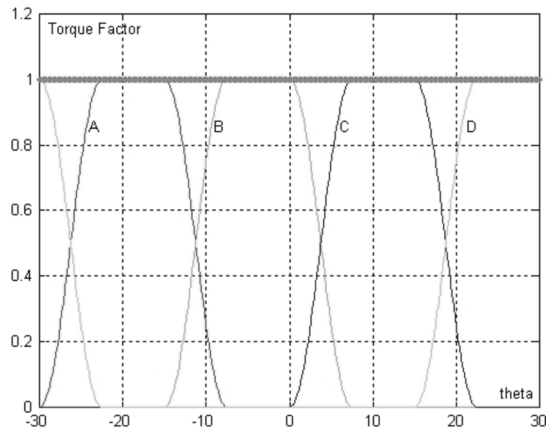

Fig. 5. Torque factors for forward-motoring operation.

the other phase is increasing. The sum of the torques generated by these phases must equal the desired torque. To determine the desired torque to be produced by each phase, torque factors are introduced here, which are defined as

$$\tau = \sum_{j=1}^{N} \tau_j \; = \; \sum_{j=1}^{N} f_j(\theta)\tau_{\text{ref}} \tag{40}$$

where $f_j(\theta)$ is the torque factor for phase j at rotor position θ and $\tau_{\text{ref}} = \tau^*$ is the desired torque. The desired torque τ^*

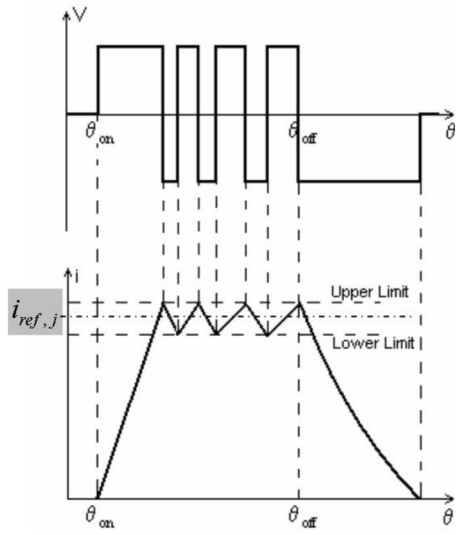

Fig. 6. Voltage and current waveforms in hysteresis current control.

was designed as shown in (22) via robust backstepping in Section III-A and can be slightly generalized analogous to (36) to be of the form

$$\tau^* = -K_p(F - F_{\text{ref}}) - K_d(\dot{F} - \dot{F}_{\text{ref}}) - K_i \int_0^t (F(t_1) - F_{\text{ref}}(t_1))\,\mathrm{d}t_1 - K_\omega \omega. \tag{41}$$

In this paper, the torque factors defined in (42), shown at the bottom of this page, are adopted. The turn-on/turn-off angles ($\theta_{\text{on},j}$ and $\theta_{\text{off},j}$) for phase A in different operating quadrants are chosen as shown in Table I. The turn-on/turn-off angles for the other phases can be obtained by phase shifting by a multiple of $(\pi/12)$.

The torque factors for all four phases in forward-motoring operation are shown in Fig. 5, where it is shown that the summation of all the four torque factors (shown by the thick dotted line) is one for any rotor position. Once the torque factors are chosen, the torque needed to be generated in each phase at any specified rotor position can be determined by multiplying the torque factor with the corresponding torque command. Then, the reference current for each phase can be computed, and phase voltages can be decided accordingly through voltage chopping—hysteresis-current-control technique (as shown in Fig. 6) will be applied to maintain the phase current within an acceptable range around the reference current.

Based on the discussed torque-control technique, a Simulink model is built to test the performance of the torque-ripple-minimizing algorithm. Here, we use a torque-ripple coefficient to measure the ripple in the torque. It is defined as

$$f_j(\theta) = \begin{cases} 0.5 - 0.5\cos(24(\theta - \theta_{\text{on},j})), & \text{if } \theta_{\text{on},j} \le \theta \le \theta_{\text{on},j} + \frac{\pi}{24} \\ 1, & \text{if } \theta_{\text{on},j} + \frac{\pi}{24} \le \theta \le \theta_{\text{off},j} - \frac{\pi}{24} \\ 0.5 + 0.5\cos\left(24\left(\theta - \theta_{\text{off},j} - \frac{\pi}{24}\right)\right), & \text{if } \theta_{\text{off},j} - \frac{\pi}{24} \le \theta \le \theta_{\text{off},j} \\ 0, & \text{otherwise.} \end{cases} \tag{42}$$

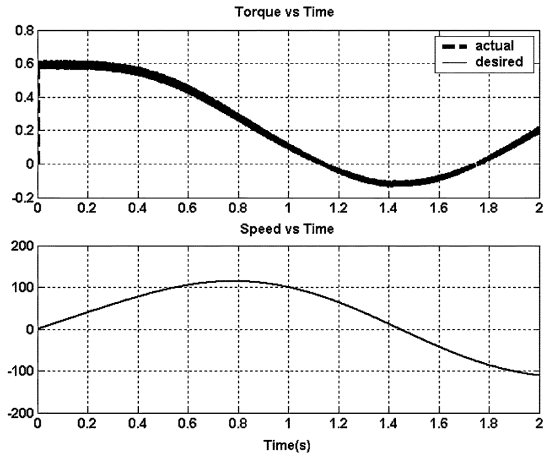

Fig. 7. Simulation results for four-quadrant torque control and torque-ripple minimization.

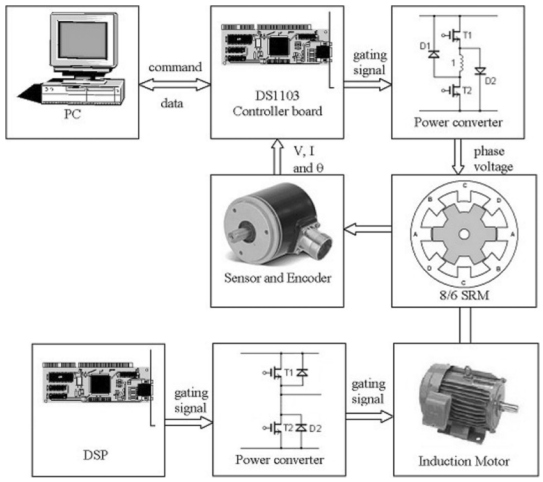

Fig. 9. Block diagram of experimental testbed.

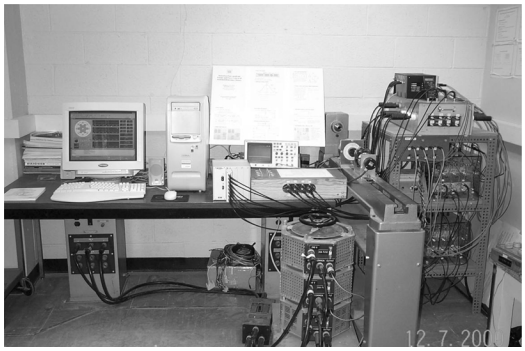

Fig. 8. Experimental setup at The Ohio State University.

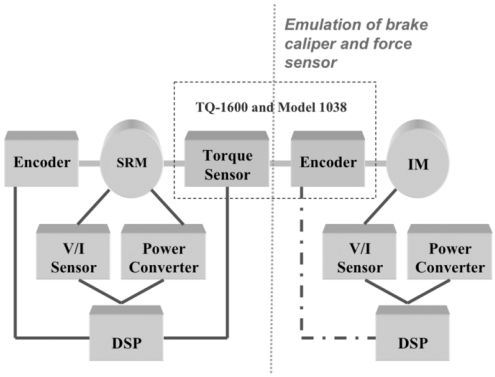

Fig. 10. Emulation of the brake caliper using IM load.

Please keep text here

$$\mathrm{TR} = \frac{\sqrt{\frac{1}{\tau_1}\int_{t_0}^{t_0+\tau_1}[\tau(t)-\tau_{\mathrm{ave}}]^2 \mathrm{d}t}}{\tau_{\mathrm{ave}}} \times 100\% \qquad (43)$$

where

$$\tau_{\mathrm{ave}} = \frac{1}{\tau_1}\int_{t_0}^{t_0+\tau_1} \tau(t)\mathrm{d}t \qquad (44)$$

t_0 is the time when a phase starts to conduct, and $t_0+\tau_1$ is the time when the next phase starts to conduct. For an 8/6 SRM, we have $\theta(t_0+\tau_1)-\theta(t_0)=(\pi/12)$.

Simulation results for four-quadrant torque control and torque-ripple minimization are shown in Fig. 7. The upper plot in Fig. 7 shows the torque command (solid line) and actual torque generated by the SRM (dashed line). The lower plot shows the rotor speed. Operation in all four quadrants is shown in Fig. 7, and it is shown that the torque ripple in all operating regions is less than 4%, which is very satisfactory.

Remark 1: The two controllers proposed in this paper each feature various controller parameters that can be tuned. The robust-backstepping control law given by (36)–(38) contains the following parameters which are free to be tuned: K_p, K_d, K_i, K_τ, K_ω, and K_{cur}. From the design in Sections III-A and III-B, it is apparent that the parameters K_p, K_d, and K_i can be interpreted as the gains in an inner loop PID controller, implying that the effects of changes in these parameters can be understood in the usual PID context (in terms of overshoot, rise time, steady-state error, etc.) and tuned using the standard PID tuning procedures. K_τ and K_ω provide damping effects and tend to slow down the response and reduce overshoots while K_{cur} affects the response time of the electrical dynamics. The robust-backstepping-based torque-level control law in conjunction with the torque-ripple-minimizing control law described in Sections III-A and III-C allows the designer to pick the parameters K_p, K_d, K_i, and K_ω and the torque factors $f_j(\theta)$. The interpretation of the parameters K_p, K_d, K_i, and K_ω is analogous to that in the case of the robust-backstepping controller as described earlier. As described in Section III-C, any choice of the torque factors which meets the requirements that the torque factors sum up to one for any rotor position and that when two phases are overlapped, the required torque should be decreasing in one phase and increasing in the other phase can be used. Appropriately chosen torque factors such as those given by (42) and Table I facilitate the current-level control and produce satisfactory torque output with a low torque ripple and low mechanical noise.

IV. Experimental Setup

A DSP-based experimental testbed (see Fig. 8) for the electromechanical brake system has been constructed in the Mecha-

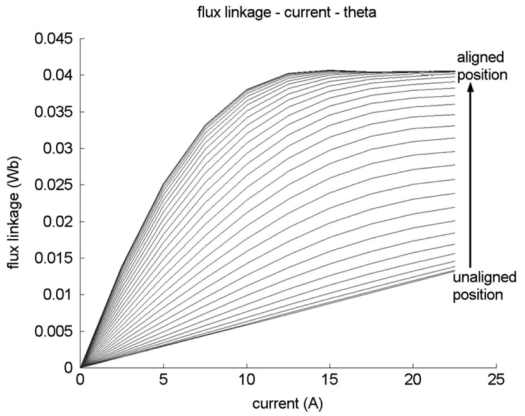

Fig. 11. Flux profile obtained from standstill-test results.

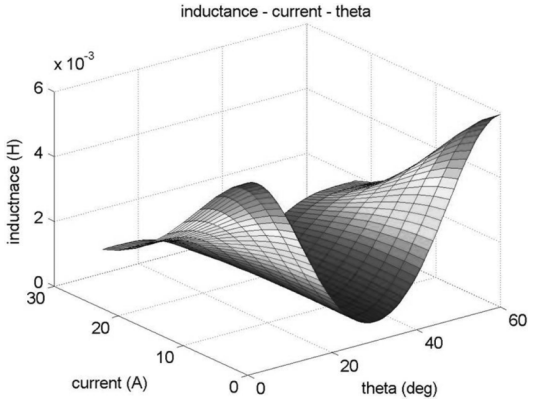

Fig. 12. Inductance profile obtained from standstill-test results.

tronics Laboratory of The Ohio State University. A block diagram of the testbed is shown in Fig. 9. The testbed contains an SRM and an induction motor (IM) which serves as the load for the SRM. Since an actual brake caliper and a clamping-force sensor were only available for preliminary testing and since the experimental results obtained with the brake caliper cannot be included in this paper due to confidentiality requirements owing to the proprietary nature of the brake caliper, an IM is used to simulate the caliper load, and a "virtual" force sensor is implemented in a DSP to simulate the force sensor as shown in Fig. 10. From experimental data, it is observed that the brake is characterized as

$$F = 2.5\Big[((1.19\times 10^{16}\hat{\theta} - 4.235\times 10^{13})\hat{\theta} + 5.904\times 10^{10})\hat{\theta} + 1.43\times 10^{6}\Big]\hat{\theta} \quad (45)$$

$$\hat{\theta} = \frac{\theta}{28}\left(\frac{0.00125}{\pi}\right) \quad (46)$$

$$\tau_L = \frac{F}{2.5}\frac{1}{28}\left(\frac{0.00125}{\pi}\right) \quad (47)$$

where $\hat{\theta}$ is the linear movement of the brake pad. The relation (46) is obtained from the gear and rotary-to-linear mechanism while (45) is the force characteristic of the caliper. The gain of the force transducer is 2.5. It may be noted that similar polynomial-based models of the clamping force have been considered previously in the literature [34]–[36].

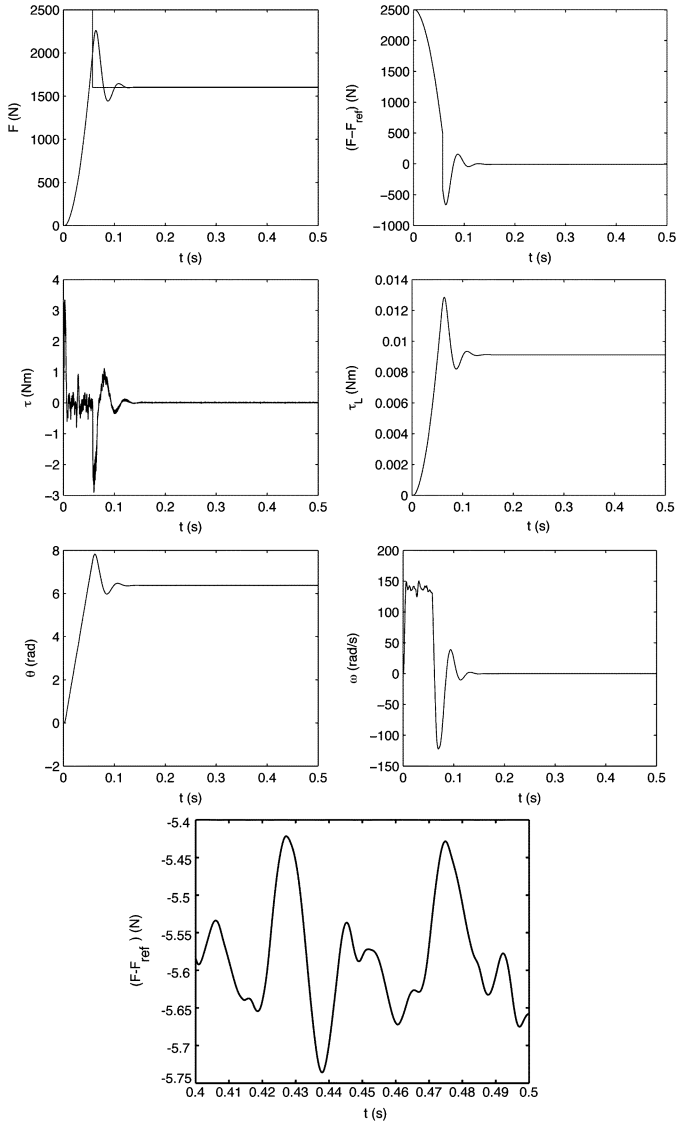

Fig. 13. Simulation results with the robust-backstepping controller. F, $F - F_{\rm ref}$, τ, τ_L, θ, ω, and steady-state $F - F_{\rm ref}$.

The virtual force sensor takes the angular movement of the rotor as input and computes the clamping force according to (45) and (46) to emulate the brake-caliper characteristic. However, while the IM load does capture the salient dynamic characteristics of a brake-caliper load, the exact load parameters and the dynamic response of the resulting closed-loop system would indeed be different as can be seen by comparing the tuned controller parameters and the dynamic response obtained in experimental tests described in Section VI with those in simulation studies discussed in Section V. A precisely calibrated torque sensor is shaft coupled in between the SRM and the induction machine. Both motor drives are DSP based and contain a power converter, a position encoder, and voltage and current sensors. The DSP system used for the SRM drive is a dSPACE DS1103 controller board system which contains two CPUs, a Motorola Power PC 604e and a TI TMS320F240 DSP. The DS1103 provides interfaces in MATLAB/Simulink to access the hardware and software systems of the controller board. The DSP system used for the IM drive is a dSPACE DS1102 control system.

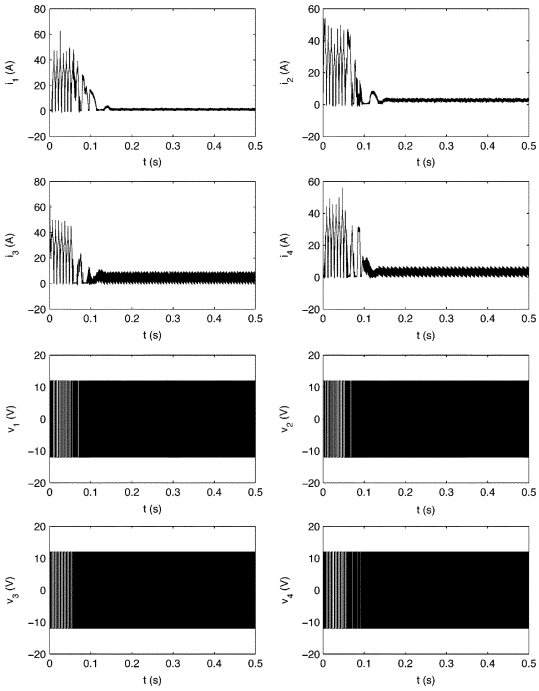

Fig. 14. Simulation results with the robust-backstepping controller: Currents and voltages.

The parameters of the SRM which comprises the actuator component in the experimental testbed shown in Fig. 8 were estimated to be $J = 7.5 \times 10^{-5}$ kg $\cdot$ m^2, $D = 0$ kg $\cdot$ m$^2/s$, $N_r = 6$, $N = 4$, $R = 0.015\,\Omega$, and $L_u = 0.13$ mH. Using the standstill test, flux as a function of current and position (see Fig. 11) and the inductance as a function of current and position (see Fig. 12) were obtained. The first five powers of the currents are included in the inductance coefficients, i.e., $k = 5$. The inductance coefficients $a_0, \ldots, a_5$, $b_0, \ldots, b_5$ were obtained using the standstill-test results and maximum-likelihood estimation to be $a_0 = 0.0009588506869$ H, $a_1 = -0.43690574 \times 10^{-5}$ H/A, $a_2 = 0.6471747 \times 10^{-6}$ H/A^2, $a_3 = -0.273123992 \times 10^{-7}$ H/A^3, $a_4 = 0.3648078578 \times 10^{-9}$ H/A^4, $a_5 = -0.1589330632 \times 10^{-11}$ H/A^5, $b_0 = 0.0004422627795$ H, $b_1 = -0.1368487 \times 10^{-5}$ H/A, $b_2 = 0.163249422 \times 10^{-6}$ H/A^2, $b_3 = -0.595375858 \times 10^{-8}$ H/A^3, $b_4 = 0.7181160145 \times 10^{-10}$ H/A^4, and $b_5 = -0.2897464391 \times 10^{-12}$ H/A^5.

V. Simulation Results

In this section, the performance of the proposed voltage-level clamping-force-control schemes is verified through simulation studies with the SRM parameters given in Section IV. The force reference trajectory is defined as follows: The force reference is 2500 N from initialization time till the time that the actual clamping force first reaches 2000 N, after which time, the force reference drops to and remains at 1600 N. The voltages are constrained to take on one of two values ± 12 V. The currents are constrained to be maintained in the range of [0, 65] A. The value $i_{\max}$ at which the control law switches to the current regulation controller (39) is picked to be 60 A.

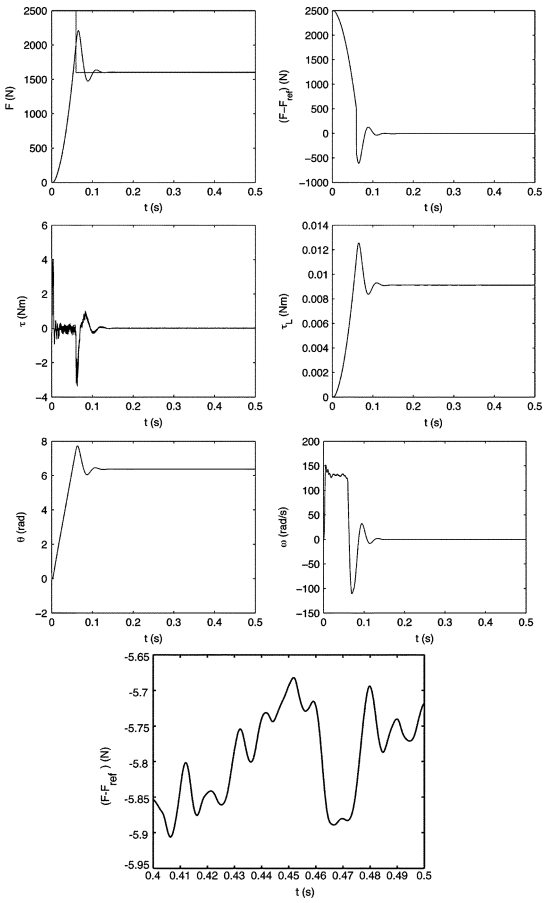

Fig. 15. Simulation results with the robust-backstepping controller (robustness analysis). F, $F - F_{\rm ref}$, τ, τ_L, θ, ω, and steady-state $F - F_{\rm ref}$.

Simulation results with the robust-backstepping-based voltage-level controller described in Sections III-A and III-B are shown in Figs. 13 and 14. The parameters of the controller were chosen to be $K_p = 30$, $K_d = 0.002$, $K_i = 2$, $K_\tau = 3500$, $K_\omega = 85$, and $K_{\rm cur} = 1$. The force, force tracking error, generated electromechanical torque, load torque, position, velocity, and a time segment of the steady-state force tracking error are shown in Fig. 13. The currents and voltages are shown in Fig. 14. It is shown that the current and voltage constraints are maintained. Both the transient and the steady-state performance are good with the average steady-state error being around 5.6 N.

To demonstrate the robustness of the controller, we consider the case in which only the constant term in the inductance expressions is available for use in the controller. The plant simulation model incorporates five powers of currents as discussed in Section IV. Retaining only the constant term in the inductance expression corresponds to maximum (attained when current = 65 A) errors of 66.3% and 25% in $L_{a,j}(i_j)$ and $L_{m,j}(i_j)$, respectively. Furthermore, the load is changed to include a cascaded first-order linear block with gain 1.1 and time constant of 2 ms. The simulation results are shown in Fig. 15. It is shown that the performance is retained (with the average steady-state error slightly increased to 5.8 N) in spite of the mismatch of inductances and unmodeled dynamic effects in the load. For

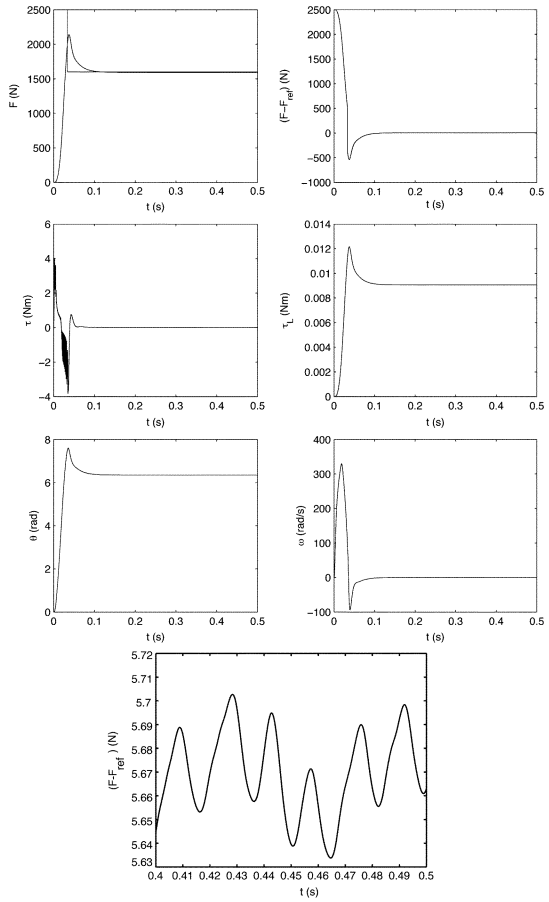

Fig. 16. Simulation results with the torque-ripple-minimizing controller. F, $F - F_{\rm ref}$, τ, τ_L, θ, ω, and steady-state $F - F_{\rm ref}$.

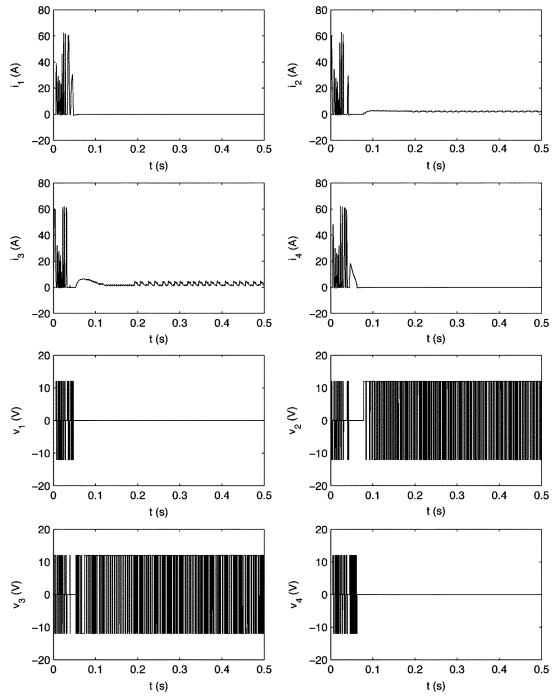

Fig. 17. Simulation results with the torque-ripple-minimizing controller: Currents and voltages.

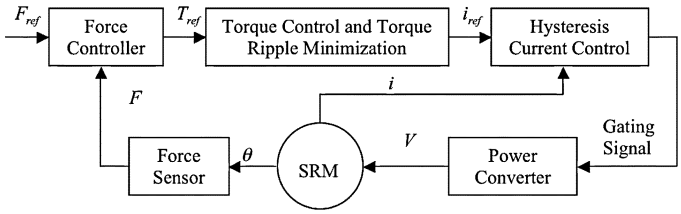

Fig. 18. Block diagram of clamping-force controller.

brevity, the current and voltage plots are not shown but are similar to the previous case.

Simulation results with the torque-ripple-minimizing algorithm (described in Section III-C) alternative to the backstepping step from torque to voltages are shown in Figs. 16 and 17. The simulations include the cascaded first-order linear block with gain 1.1 and time constant 2 ms in the load described earlier. The controller parameters were chosen to be $K_p = 0.0016$, $K_d = 0.00004$, $K_i = 0.00001$, and $K_\omega = 0.001$. The torque factors are chosen as given by (42) and Table I. It is shown that the performance is comparable to that of the robust-backstepping controller (see Fig. 15).

VI. Experimental Results

As described in Section IV, a DSP-based experimental testbed (see Fig. 8) for the electromechanical brake system has been constructed in the Mechatronics Laboratory of The Ohio State University. The four-quadrant torque control and torque-ripple-minimizing algorithm (see Section III-C) has been implemented in the DSP to convert the torque command obtained from the robust-backstepping controller in Section III-A to phase-voltage commands. A block diagram of the controller is shown in Fig. 18. The force reference trajectory is defined as in the simulation studies, i.e., the force reference is initially 2500 N; when the actual clamping force reaches 2000 N, the force reference command drops to and remains at 1600 N.

The controller parameters are chosen as $K_p = 0.0135$, $K_d = 0.0$, $K_i = 2.7 \times 10^{-8}$, and $K_\omega = 0.24$. The torque factors are chosen as given by (42) and Table I. The experimental results are shown in Figs. 19–21. In Fig. 19, the clamping-force response is shown along with force tracking error. The four-quadrant torque–speed curve is shown in Fig. 20, and it is shown that the torque ripple is small. The phase voltages and currents are shown in Fig. 21. The steady-state force response is 1659.6 N, i.e., the steady-state force tracking error is 59.6 N (which corresponds to 3.7% of the force reference). The steady-state tracking error can be reduced at the expense of a higher transient overshoot by increasing the parameters K_p and K_i.

VII. Conclusion

We proposed robust nonlinear force controllers for an SRM-based electromechanical brake system. A detailed model of the motor including current dependence of the inductance coefficients was used. The load was taken to be an unknown nonlinear function of position. A torque-level control law was designed via a robust-backstepping procedure. Two schemes to obtain voltage-level control laws from the torque-level control

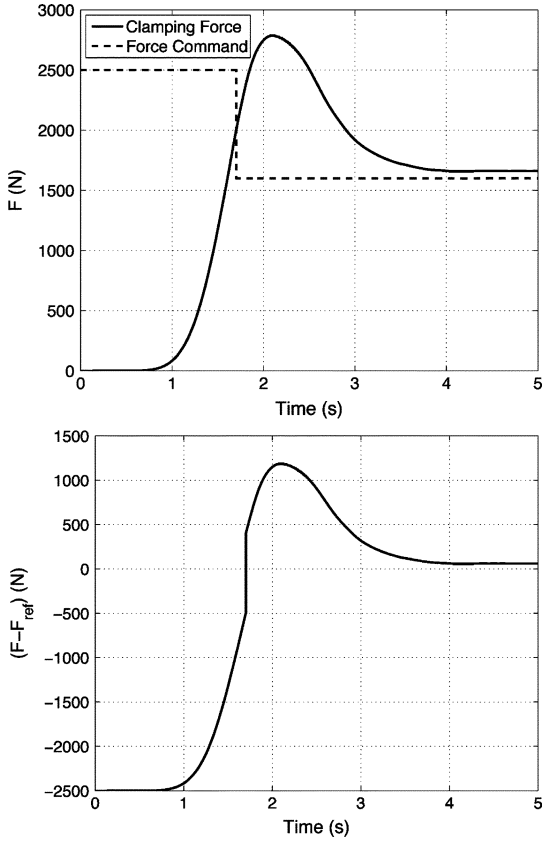

Fig. 19. Experimental results: Clamping-force response.

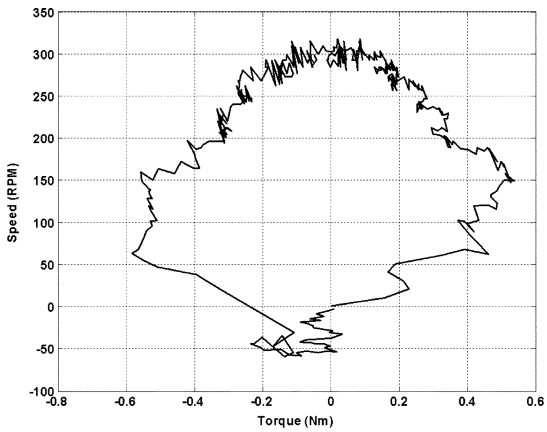

Fig. 20. Experimental results: Four-quadrant torque–speed curve.

law were proposed, one based on an additional step of robust backstepping and another based on torque ripple minimization. The proposed controllers provide four-quadrant operation (i.e., support forward- and backward-motoring and braking regimes of operation). The controllers do not require knowledge of the motor mechanical parameters and the functional forms of the relationships among motor position, brake force, and motor load torque. Moreover, the controllers provide significant robustness to uncertainty in the inductances. The proposed controller design can also be extended to brake systems using other types of motors. Implementation issues including current

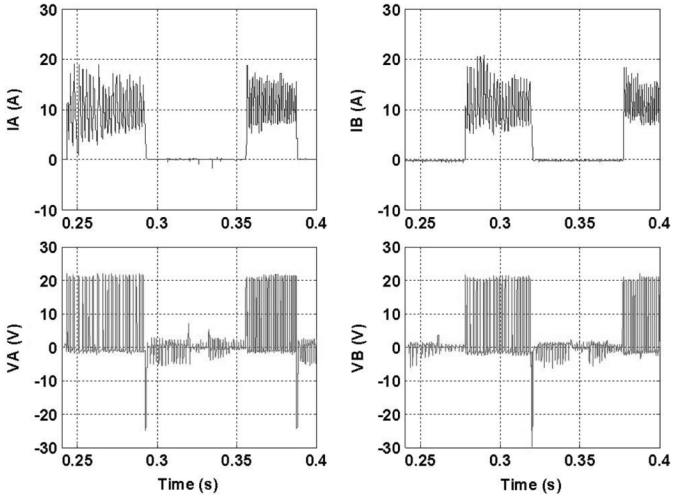

Fig. 21. Experimental results: Phase voltage and current waveforms.

and voltage constraints were also addressed. The performance and robustness of the proposed controllers were demonstrated through simulation and experimental studies.

REFERENCES

[1] E. A. Bretz, "By-wire cars turn the corner," *IEEE Spectr.*, vol. 38, no. 4, pp. 68–73, Apr. 2001.
[2] R. Schwarz, R. Isermann, J. Bohm, J. Nell, and P. Rieth, "Modeling and control of an electromechanical disk brake," presented at the Society Automotive Engineering (SAE) Technical Paper Series 980600, Int. Congr. and Expo., Detroit, MI, Feb. 1998.
[3] M. Gunzert and A. Nagele, "Component-based development and verification of safety critical software for a brake-by-wire system with synchronous software components," in *Proc. Int. Symp. Softw. Eng. Parallel Distrib. Syst.*, Los Angeles, CA, May 1999, pp. 134–145.
[4] M. Kees, K. J. Burnham, F. P. Lockett, J. H. Tabor, and R. A. Williams, "Hydraulic actuated brake and electromechanically actuated brake systems," in *Proc. IEE Int. Conf. ADAS*, Sep. 2001, pp. 43–47.
[5] M. Bodson, "Trends in electronics for electric motor control," *IEEE Control Syst. Mag.*, vol. 16, no. 5, pp. 88–96, Oct. 1996.
[6] R. B. Inderka, M. Menne, and R. W. A. A. De Doncker, "Control of switched reluctance drives for electric vehicle applications," *IEEE Trans. Ind. Electron.*, vol. 49, no. 1, pp. 48–53, Feb. 2002.
[7] K. M. Rahman and S. E. Schulz, "Design of high-efficiency and high-torque-density switched reluctance motor for vehicle propulsion," *IEEE Trans. Ind. Appl.*, vol. 38, no. 6, pp. 1500–1507, Nov./Dec. 2002.
[8] J. Faiz and J. W. Finch, "Aspects of design optimisation for switched reluctance motors," *IEEE Trans. Energy Convers.*, vol. 8, no. 4, pp. 704–713, Dec. 1993.
[9] Y. Tang, "Characterization, numerical analysis, and design of switched reluctance motors," *IEEE Trans. Ind. Appl.*, vol. 33, no. 6, pp. 1544–1552, Nov./Dec. 1997.
[10] B. Fahimi, G. Suresh, and M. Ehsani, "Design considerations of switched reluctance motors: Vibration and control issues," in *Proc. Ind. Appl. Conf.*, Phoenix, AZ, Oct. 1999, pp. 2259–2266.
[11] B. Fahimi, G. Suresh, J. Mahdavi, and M. Ehsani, "A new approach to model switched reluctance motor drive application to dynamic performance prediction, control and design," in *Proc. Electron. Spec. Conf.*, May 1998, pp. 2097–2102.
[12] S. Mir, I. Husain, and M. E. Elbuluk, "Switched reluctance motor modeling with on-line parameter identification," *IEEE Trans. Ind. Appl.*, vol. 34, no. 4, pp. 776–783, Jul./Aug. 1998.
[13] N. J. Nagel and R. D. Lorenz, "Modeling of a saturated switched reluctance motor using an operating point analysis and the unsaturated torque equation," *IEEE Trans. Ind. Appl.*, vol. 36, no. 3, pp. 714–722, May/Jun. 2000.
[14] B. C. Mecrow, C. Weiner, and A. C. Clothier, "The modeling of switched reluctance machines with magnetically coupled windings," *IEEE Trans. Ind. Appl.*, vol. 37, no. 6, pp. 1675–1683, Nov./Dec. 2001.

[15] I. Moson, K. Iwan, and J. Nieznanski, "Circuit-oriented model of the switched reluctance motor for drive systems simulation," in *Proc. IEEE Annu. Conf. Ind. Electron. Soc.*, Nov. 2002, pp. 497–501.
[16] W. Lu, A. Keyhani, and A. Fardoun, "Neural network-based modeling and parameter identification of switched reluctance motors," *IEEE Trans. Energy Convers.*, vol. 18, no. 2, pp. 284–290, Jun. 2003.
[17] M. Ilic'-Spong, R. Marino, S. Peresada, and D. G. Taylor, "Feedback linearizing control of switched reluctance motors," *IEEE Trans. Autom. Control*, vol. AC-32, no. 5, pp. 371–379, May 1987.
[18] D. Taylor, "An experimental study on composite control of switched reluctance motors," *IEEE Control Syst. Mag.*, vol. 11, no. 2, pp. 31–36, Feb. 1991.
[19] J. Carroll and D. Dawson, "Adaptive tracking control of a switched reluctance motor turning an inertial load," in *Proc. Am. Control Conf.*, San Francisco, CA, Jun. 1993, pp. 670–674.
[20] R. R. Kohan and S. A. Bortoff, "Adaptive control of variable reluctance motors using spline functions," in *Proc. IEEE Conf. Decision Control*, Lake Buena Vista, FL, Dec. 1994, pp. 1694–1699.
[21] D. Dawson, J. Hu, and T. Burg, *Nonlinear Control of Electric Machinery*. New York: Marcel Dekker, 1998.
[22] H. Melkote, F. Khorrami, S. Jain, and M. Mattice, "Robust adaptive control of variable reluctance stepper motors," *IEEE Trans. Control Syst. Technol.*, vol. 7, no. 2, pp. 212–221, Mar. 1999.
[23] J. Chiasson and L. Tolbert, "High performance motion control of a switched reluctance motor," in *Proc. IEEE Elect. Mach. Drives Conf.*, Cambridge, MA, Jun. 2001, pp. 425–429.
[24] F. Khorrami, P. Krishnamurthy, and H. Melkote, *Modeling and Adaptive Nonlinear Control of Electric Motors*. New York: Springer-Verlag, 2003.
[25] G. Espinosa-Perez, P. Maya-Ortiz, M. Velasco-Villa, and H. Sira-Ramirez, "Passivity-based control of switched reluctance motors with nonlinear magnetic circuits," *IEEE Trans. Control Syst. Technol.*, vol. 12, no. 3, pp. 439–448, May 2004.
[26] N. C. Sahoo, J. X. Xu, and S. K. Panda, "Low torque ripple control of switched reluctance motors using iterative learning," *IEEE Trans. Energy Convers.*, vol. 16, no. 4, pp. 318–326, Dec. 2001.
[27] W. Yan, Y. Tianming, F. Yu, and L. Guoguo, "Intelligent control for torque ripple minimization of SRM," in *Proc. Int. Conf. Elect. Mach. Syst.*, Nanjing, China, Sep. 2005, pp. 742–747.
[28] K. M. Rahman, S. Gopalakrishnan, B. Fahimi, A. V. Rajarathnam, and M. Ehsani, "Optimized torque control of switched reluctance motor at all operational regimes using neural network," *IEEE Trans. Ind. Appl.*, vol. 37, no. 3, pp. 904–913, May/Jun. 2001.
[29] A. A. Goldenberg, I. Laniado, P. Kuzan, and C. Zhou, "Control of switched reluctance motor torque for force control applications," *IEEE Trans. Ind. Electron.*, vol. 41, no. 4, pp. 461–466, Aug. 1994.
[30] I. Kioskeridis and C. Mademlis, "Maximum efficiency in single-pulse controlled switched reluctance motor drives," *IEEE Trans. Energy Convers.*, vol. 20, no. 4, pp. 809–817, Dec. 2005.
[31] F.-C. Lin and S.-M. Yang, "Modeling and control of radial force in switched reluctance motor," in *Proc. IEEE Power Electron. Spec. Conf.*, Jeju, Korea, Jun. 2006, pp. 1–7.
[32] R. A. McCann, M. S. Islam, and I. Husain, "Application of a sliding-mode observer for position and speed estimation in switched reluctance motor drives," *IEEE Trans. Ind. Appl.*, vol. 37, no. 1, pp. 51–58, Jan./Feb. 2001.
[33] M. Krstić, I. Kanellakopoulos, and P. V. Kokotović, *Nonlinear and Adaptive Control Design*. New York: Wiley, 1995.
[34] R. Schwarz, R. Isermann, J. Bohm, J. Nell, and P. Rieth, "Clamping force estimation for a brake-by-wire actuator," presented at the Society Automotive Engineering (SAE) Technical Paper Series 990482, Int. Congr. and Expo., Detroit, MI, Mar. 1999.
[35] S. Saric, A. Bab-Hadiashar, and R. Hoseinnezhad, "A sensor fusion approach to estimate clamp force in brake-by-wire systems," in *Proc. IEEE Veh. Technol. Conf.*, Melbourne, Australia, May 2006, pp. 3007–3011.
[36] R. Hoseinnezhad, A. Bab-Hadiashar, and T. Rocco, "Real-time clamp force measurement in electromechanical brake calipers," *IEEE Trans. Veh. Technol.*, vol. 57, no. 2, pp. 770–777, Mar. 2008.

Prashanth Krishnamurthy (S'01–M'06) received the B.Tech. degree in electrical engineering from the Indian Institute of Technology, Chennai, India, in 1999 and the M.S. and Ph.D. degrees in electrical engineering from the Polytechnic University, Brooklyn, NY, in 2002 and 2006, respectively.

He is currently a Senior Electrical Engineer with IntelliTech Microsystems, Inc., Bowie, MD. He has coauthored over 50 journal and conference papers and the book "Modeling and Adaptive Nonlinear Control of Electric Motors" (Springer–Verlag, 2003). His research interests include robust and adaptive nonlinear control with applications to electromechanical systems, large-scale systems, and unmanned vehicles.

Wenzhe Lu (S'00–M'05) received the B.S. degree from Xi'an Jiaotong University, Xi'an, China, in 1993, the M.S. degree from Tsinghua University, Beijing, China, in 1996, and the Ph.D. degree from The Ohio State University, Columbus, in 2005.

He is currently a Power and Controls Engineer with Vanner Inc., Hilliard, OH. His research interests include power conversion and control devices and motor drives for vehicle applications.

Farshad Khorrami (S'85–M'88–SM'96) was born in Iran on January 22, 1962. He received the B.S. degree in mathematics, the B.S. degree in electrical engineering, the M.S. degree in mathematics, and the Ph.D. degree in electrical engineering from The Ohio State University, Columbus, in 1982, 1984, 1984, and 1988, respectively.

He is currently a Professor of electrical and computer engineering with the Polytechnic University, Brooklyn, NY, where he was an Assistant Professor since September 1988 and has developed and directed the Control/Robotics Research Laboratory, Department of Electrical and Computer Engineering. He has published more than 180 refereed journal and conference papers. He is also an author of a recently published book entitled *Modeling and Adaptive Nonlinear Control of Electric Motors* (Springer–Verlag, 2003). He is the holder of 12 U.S. patents. His research interests include adaptive and nonlinear control, electromechanical systems modeling and control, large-scale systems and decentralized control, unmanned autonomous vehicles, smart structures, robotics and high-speed positioning application, and microprocessor-based control and instrumentation.

Dr. Khorrami has served on the program committees of several conferences and has been a member of the Conference Editorial Board of the Control Systems Society. He is the Industrial Chair of the 2009 IEEE Multi-conference on Systems and Control.

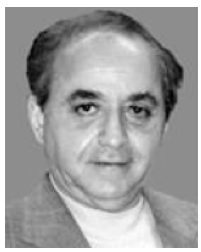

Ali Keyhani (F'98) From 1967 to 1972, he was with Hewlett-Packard Company and TRW Control. He is currently a Professor of electrical engineering with the Department of Electrical and Computer Engineering, The Ohio State University, Columbus, where he is also the Director of OSU Mechatronic–Green Energy Systems Laboratory. His current research activities focus on the integration and control of renewable and green energy in distributed energy systems, power electronics, multilevel converters, power systems control, alternative energy systems, fuel cells, photovoltaic cells, microturbines, distributed generation systems, and parameter estimation and control of electromechanical systems.

Prof. Keyhani was the past Chairman of the Electric Machinery Committee of the IEEE Power Engineering Society. He was the past Editor of the IEEE TRANSACTIONS ON ENERGY CONVERSION. He was the recipient of The Ohio State University College of Engineering Research Award for 1989, 1999, and 2003.